ACS SENSORS

pubs.acs.org/acssensors

Article

Quantum Dot Lipase Biosensor Utilizing a Custom-Synthesized Peptidyl-Ester Substrate

Joyce C. Breger, Kimihiro Susumu, Guillermo Lasarte-Aragonés, Sebastián A. Díaz, Jesper Brask, and Igor L. Medintz*

Cite This: https://dx.doi.org/10.1021/acssensors.9b02291

Read Online

ACCESS | Metrics & More | Article Recommendations | Supporting Information

ABSTRACT: Lipases are an important class of lipid hydrolyzing enzymes that play significant roles in many aspects of cell biology and digestion; they also have large roles in commercial food and biofuel preparation and are being targeted for pharmaceutical development. Given these, and many other biotechnological roles, sensitive and specific biosensors capable of monitoring lipase activity in a quantitative manner are critical. Here, we describe a Förster resonance energy transfer (FRET)-based biosensor that originates from a custom-synthesized ester substrate displaying a peptide at one end and a dye acceptor at the other. These substrates were ratiometrically self-assembled to luminescent semiconductor quantum dot (QD) donors by metal affinity coordination using the appended peptide's terminal hexahistidine motif to give rise to the full biosensing construct. This resulted in a high rate of FRET between the QD donor and the proximal substrate's dye acceptor. The lipase hydrolyzed the intervening target ester bond in the peptide substrate which, in turn, displaced the dye acceptor containing component and altered the rate of FRET in a concentration-dependent manner. Specifics of the substrate's stepwise synthesis are described along with the sensors assembly, characterization, and application in a quantitative proof-of-concept demonstration assay that is based on an integrated Michaelis−Menten kinetic approach. The utility of this unique nanoparticle-based architecture within a sensor configuration is then discussed.

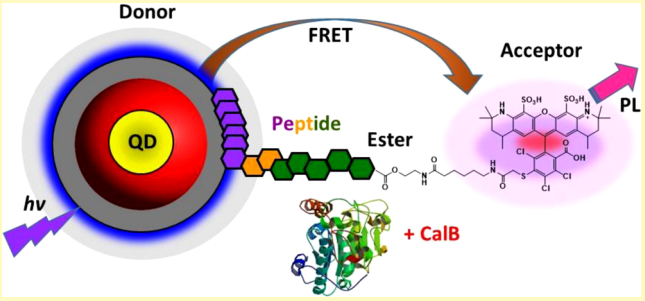

KEYWORDS: *lipase, enzyme, quantum dot, FRET, esterase, nanotechnology, biosensor*

INTRODUCTION

The exponential growth of synthetic biology serves to reinforce how important it is to have the capability to fully characterize and quantitate the activity of a given enzyme for it to be fully exploited in subsequent applications.[1] Lipases are an important class of lipid hydrolyzing enzymes whose application outside of their classic roles in cell biology, food digestion, and the virulence of select pathogens such as *Candida albicans*, epitomize increasing commercial interest in biocatalyzed chemical conversion and similar processes.[2,3] Lipases are now critical in industrial food preparation such as baking and vegetable oil processing, pretreatment of cellulosic feedstocks in second-generation (bio)fuel preparation, and as additives in many detergents; they are also now commonly added to animal feed to help with digestion.[4,5] Their primary purpose in almost all these applications is to break down or hydrolyze complex lipids into more manageable components that can be removed, digested, or further processed. As their contributions in more complex physiological processes are elucidated, lipases are also becoming attractive as potential druggable pharmaceutical targets.[6] Despite their wide diversity, the common element in almost all these applications is the requirement for sensitive and specific assays that can monitor lipase activity and this is increasingly being provided for other types of hydrolytic enzymes by nanoparticle (NP)-based biosensors.[7]

Lipases are part of the family of esterases, with both considered to be under the superfamily of carboxylesterases; the distinction is based on their substrate specificity with lipases distinguished by their ability to hydrolyze insoluble long-chain triacylglycerols and soluble short acyl chain esters, while esterases are typically capable of only acting on the latter.[8] As a scaffolding material to host lipase substrate(s), NPs are attractive since they provide access to a unique combination of features that are not easily found in a fluorescent, chromogenic, or radiolabeled single molecular entity lipidic substrate. These include the ability to host and display multiple copies of substrate molecules in a dense, localized format that is reminiscent of how lipids appear at an interface.[9] Moreover, in the right configuration, NPs can potentially stabilize the colloidal display of long-chain or

Received: November 19, 2019
Accepted: February 7, 2020

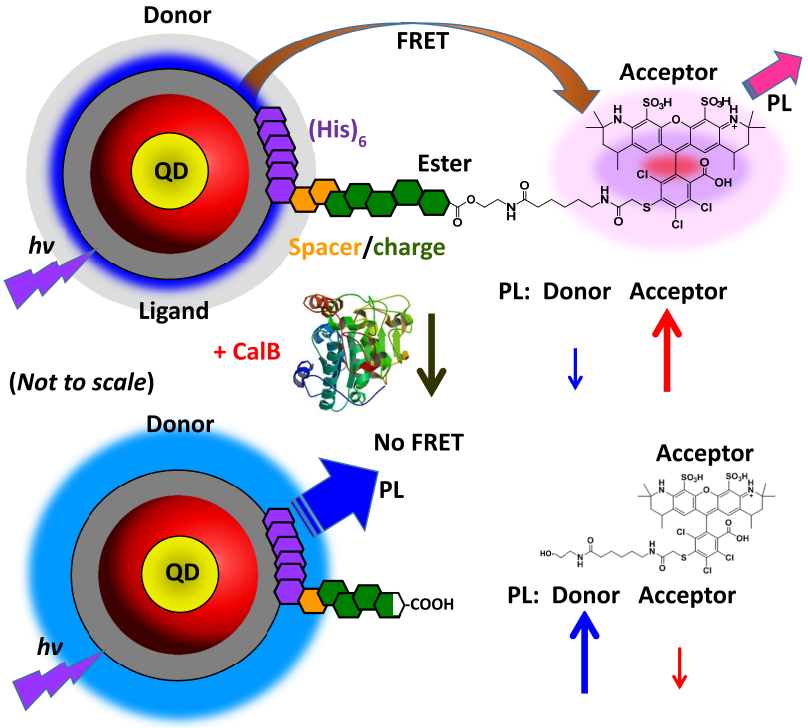

Figure 1. Schematic of the QD-lipase biosensor. The sensor consists of 520 nm emitting CdSe/CdZnS/ZnS core/shell/shell QDs ratiometrically self-assembled with ester-containing peptidyl substrate conjugates. The central QD acts as an energy donor and assembly scaffold for displaying the ester substrates. The substrate consists of a modular peptide displaying a $(His)_6$ for metal affinity coordination to the QD surface, an extended spacer, and then a charged sequence. Appended to this is the target ester recognized and cleaved by the lipase and then a dye acceptor. Upon excitation, the QD transfers energy to the acceptor dye by FRET resulting in a decrease in QD photoluminescence (PL) and an increase in acceptor sensitized PL. FRET efficiency can be modulated by the number of peptido-acceptors ratiometrically assembled around the QD. Lipase (CalB) cleaves the ester allowing it to diffuse away, altering FRET, decreasing acceptor sensitization, and increasing QD donor PL.

complex lipidic structures that may be insoluble in aqueous buffers on their own. Depending upon their unique physicochemical and quantum-confined properties, the incorporation of a given NP material into a biosensing configuration can allow for the exploitation of a specific signal transduction modality such as those based on magnetics, plasmonics, and fluorescence along with Förster resonance energy transfer (FRET).[10−12] In terms of FRET-based hydrolytic biosensing, luminescent semiconductor quantum dots (QDs) have been extensively used as scaffolds for the display of molecular substrates primarily targeting proteases along with some other types of enzyme activity such as transferases.[7,13,14] In this configuration, the QD acts as a central exciton donor and dye-labels or quenchers attached to the substrate act as the acceptor(s). Proteolytic activity separates the acceptor from the donor scaffold and this can often be monitored in a manner that allows the data to be converted into quantitative units of enzyme activity.[15,16] Although, this configuration should intuitively lend itself to monitoring lipase hydrolytic activity, there are almost no examples of using QDs for such FRET-based assays. In one of the only somewhat related reports, Zhang reported on a method to monitor lipase activity by following its cleavage of a metallic precursor containing substrate that led to the growth of fluorescent QDs.[17] Here, we show proof-of-concept for a prototypical QD-based lipase hydrolytic sensor that functions via FRET. The design and function of the sensor are schematically highlighted in Figure 1. The substrate's stepwise synthesis is described in detail along with the sensors assembly, characterization, and application in a quantitative lipase assay that utilizes an integrated Michaelis−Menten (MM) kinetic approach.

MATERIALS AND METHODS

Quantum Dots, Reagents, and Lipase. CdSe/CdZnS/ZnS core/shell/shell 520 nm emitting QDs were synthesized as described.[18−20] Following synthesis, the QD's native hydrophobic surface ligand was cap-exchanged with compact ligand CL4 as described previously;[18,19] see Figure S1 in the Supporting Information (SI) for the structure of the ligand. β-Alanine, trimethylsilyl chloride, ethanolamine, and *N*,*N*-diisopropylethylamine were purchased from Sigma-Aldrich (St. Louis, MO). Trityl chloride, *N*,*N*′-dicyclohexylcarbodiimide, 4-(dimethylamino)pyridine, and trifluoroacetic acid were purchased from Acros Organics (Fisher Scientific, Pittsburgh, PA). Unless otherwise mentioned in the text, all other chemicals including solvents were purchased from Sigma-Aldrich or Acros Organics and used as received. Lipase B cloned from *Candida antarctica* (CalB) and recombinantly expressed in *Aspergillus oryzae* was obtained from Sigma-Aldrich with a specific activity of 11.8 units (U)/mg where 1 U corresponds to the amount of enzyme that functionally liberates 1 μmol of butyric acid/min at pH 8.0 and 40 °C from a tributyrin substrate. 4-Nitrophenyl palmitate (NPPL) lipase substrate was also obtained from Sigma-Aldrich.

Instrumentation. ^{1}H NMR spectra were recorded on a Bruker SpectroSpin 400 MHz spectrometer (Bruker, Billerica, MA). Chemical shifts for ^{1}H NMR spectra are reported relative to tetramethylsilane (TMS) signal in deuterated solvent (TMS, δ = 0.00 ppm). All J values are reported in hertz. The structure of the synthetic intermediaries and the final product were confirmed using an Acquity Ultra Performance Liquid Chromatography (UPLC) H-Class system equipped with an SQD2 mass detector (Waters, Milford, MA).[21,22] Electronic absorption spectra were recorded using an HP

https://dx.doi.org/10.1021/acssensors.9b02291
ACS Sens. XXXX, XXX, XXX−XXX

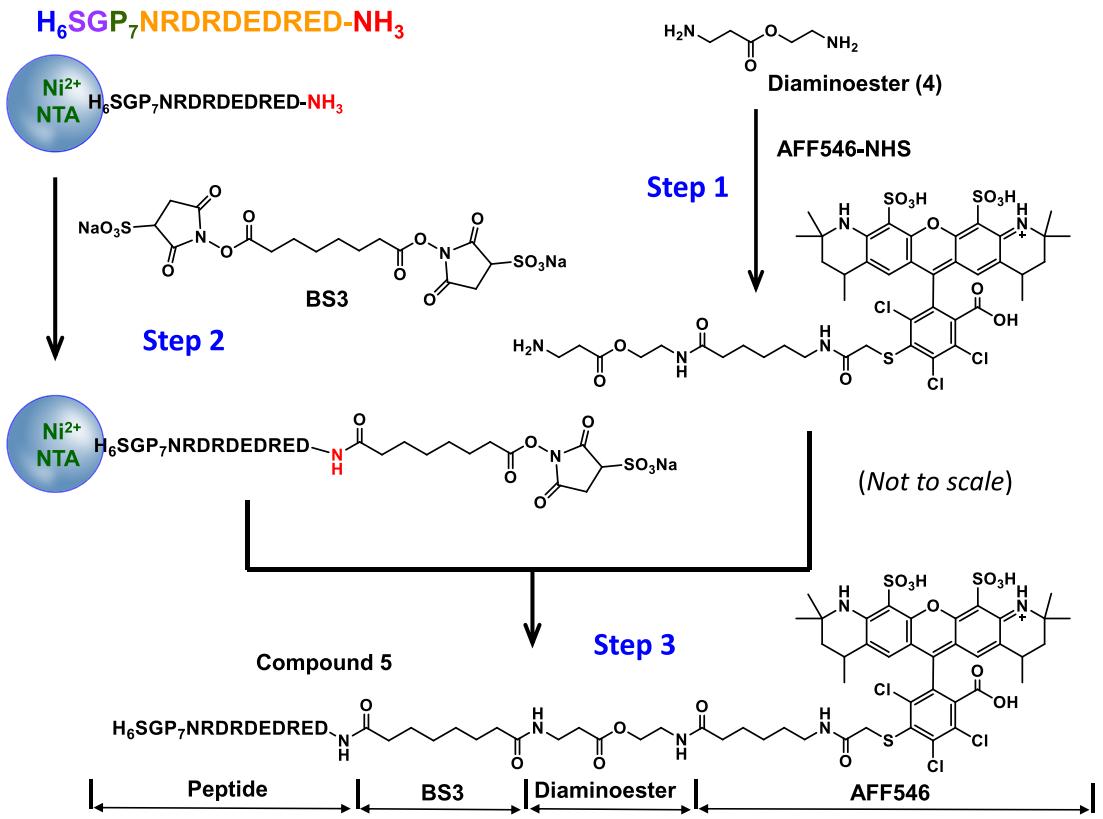

Figure 2. Assembly of the acceptor dye-labeled ester-containing peptide substrate. Step 1: The initial diaminoester (compound **4**, bis-trifluoroacetic acid salt) is first labeled with an acceptor dye on one of its constituent primary amines in a non-site-specific manner. An NHS-activated Alexa Fluor 546 dye is utilized in this case with UPLC−MS used to confirm labeling and purify the monolabeled product. Step 2: The modular, multifunctional peptide has the sequence H_6SGP$_7$NRDRDEDRED-NH_3 (shown C- to N-terminus) where the H_6 (blue) represents the QD attachment module, SG (purple) is a flexible linker, P_7 (green) a rigid type II helix, NRDRDEDRED (orange) is a charged sequence meant to mimic the cell surface, and the unique N-terminal primary amine (red) that is modified in the subsequent chemistry. The peptide is first loaded onto Ni^{2+}-NTA resin and then activated with homobifunctional BS3 on its terminal primary amine to, in turn, display a sulfo-NHS reactive group. Step 3: Following removal of excess BS3 and washing, the acceptor dye-labeled ester is passed over the BS3-activated peptide repeatedly to yield the final peptide-ester−dye substrate shown on the bottom. Correct assembly (compound **5**, shown with one of two possible configurations for the ester position) is confirmed by MS analysis and, following UPLC purification, the final product was quantitated and lyophilized. Specific details of the chemistry can be found in the Materials and Methods section.

8453 diode array spectrophotometer (Agilent Technologies, Santa Clara, CA). FRET-based enzyme assays were carried out on a Tecan Spark Microtiter Well Plate Reader (Männedorf, Switzerland).[23]

Synthesis of the Diaminoester. See Figure S1 in the SI for chemical structures of the intermediaries and the synthetic product.

*N-Trityl-3-aminopropionic Acid (**1**).* To a mixture of *β*-alanine (5.104 g, 5.73 × 10^{-2} mol) in anhydrous CH_2Cl_2 (70 mL) and CH_3CN (15 mL) was added 1.0 M solution of trimethylsilyl chloride in tetrahydrofuran (THF, 63 mL, 6.3 × 10^{-2} mol). The reaction mixture was refluxed for 1 h under N_2, then cooled to 0 °C. To the reaction mixture at 0 °C, triethylamine (17.0 mL, 0.122 mol) was added dropwise. Trityl chloride (18.0 g, 6.46 × 10^{-2} mol) was then added to the reaction mixture in three equal portions within 15 min. Stirring was continued at 0 °C for 1 h and at room temperature for 5.5 h. Methanol (MeOH, 20 mL) was introduced into the reaction mixture, which was then stirred at room temperature for 1 h, and the solvent was evaporated to dryness. 1 M NaOH solution (200 mL) was added to the residue and the aqueous solution was washed twice with diethyl ether (Et_2O). The aqueous layer was cooled in an ice-bath and brought to pH 5 by the dropwise addition of acetic acid. A 5% aqueous citric acid solution was then added to further acidify the reaction mixture until no more precipitate was formed. The precipitate was filtered, washed twice with deionized water, and dissolved in a 5:1 (v/v) mixture of $CHCl_3$/MeOH (200 mL). The product solution was dried over $MgSO_4$, filtered, and the solvent was evaporated to give product **1**. Yield = 17.813 g (94% based on 5.104 g of *β*-alanine). ^{1}H NMR (400 MHz, $CDCl_3$): *δ* 7.37−7.45 (m, 6H, Ph), 7.19−7.36 (m, 9H, Ph), 2.58 (t, 2H, *J* = 7.6 Hz, CH_2), 2.47 (t, 2H, *J* = 7.5 Hz, CH_2). Electrospray ionization (ESI) mass spectrometry (MS) *m*/*z*: 330.167 $(M - H)^-$/expected *m*/*z* value $(M - H)^-$ was 330.149.

*N-Trityl-2-aminoethanol (**2**).* Ethanolamine (4.0 mL, 6.63 × 10^{-2} mol) was added to a solution of trityl chloride (24.0 g, 8.61 × 10^{-2} mol) in CH_2Cl_2 (50 mL) cooled to 0 °C under N_2. *N*,*N*-Diisopropylethylamine (18.0 mL, 0.103 mol) was added dropwise. The reaction mixture was then gradually warmed to room temperature and stirred for 4 h. $CHCl_3$ (100 mL) was mixed in, and the reaction mixture was washed with water (2 × 50 mL) and brine (50 mL). The organic layer was dried over Na_2SO_4. The inorganic salt was filtered off and the solvent was evaporated. The residue was purified using chromatography on silica gel with $CHCl_3$, then with $CHCl_3$/MeOH (20:1). Yield = 7.365 g (37% based on 4.0 mL of ethanolamine). ^{1}H NMR (400 MHz, $CDCl_3$): *δ* 7.44−7.51 (m, 6H, Ph), 7.24−7.35 (m, 6H, Ph), 7.16−7.24 (m, 3H, Ph), 3.69 (t, 2H, *J* = 6.4 Hz, CH_2), 2.35 (t, 2H, *J* = 7.0 Hz, CH_2), 2.14 (br s, 1H). ESI MS *m*/*z*: 302.054 $(M - H)^-$/expected *m*/*z* value $(M - H)^-$ was 302.154.

*N,N′-Bis(trityl)-2′-aminoethyl-3-aminopropionate (**3**).* *N*,*N*′-Dicyclohexylcarbodiimide (2.26 g, 1.10 × 10^{-2} mol) in $CHCl_3$ (40 mL) was added dropwise to a solution of *N*-trityl-3-aminopropionic acid (**1**) (3.00 g, 9.05 × 10^{-3} mol), *N*-trityl-2-aminoethanol (**2**) (2.542 g, 8.38 × 10^{-3} mol), and 4-(dimethylamino)pyridine (0.238 g, 1.95 ×

https://dx.doi.org/10.1021/acssensors.9b02291
ACS Sens. XXXX, XXX, XXX−XXX

10^{-3} mol) in $CHCl_3$ (100 mL). The reaction mixture was stirred at room temperature for 3 days under N_2. The white precipitate was filtered off through celite, and the filtrate was evaporated. The residue was purified using chromatography on silica gel with $CHCl_3$. Yield = 5.164 g (quantitative based on 2.542 g of *N*-trityl-2-aminoethanol). ^{1}H NMR (400 MHz, $CDCl_3$): δ 7.41−7.50 (m, 12H, Ph), 7.12−7.33 (m, 18H, Ph), 4.19 (t, 2H, J = 7.3 Hz, CH_2), 2.52 (t, 2H, J = 8.2 Hz, CH_2), 2.38 (t, 4H, J = 7.4 Hz, CH_2). ESI MS m/z: 639.319 (M + Na)$^+$/expected m/z value (M + Na)$^+$ was 639.299.

2′-Aminoethyl-3-aminopropionate Bis(trifluoroacetate) Salt (4). Trifluoroacetic acid (2.0 mL, 2.6×10^{-2} mol) was added dropwise to a solution of **3** (3.422 g, 5.55×10^{-3} mol) in CH_2Cl_2 (25 mL) cooled in an ice-bath under N_2. The reaction mixture was stirred at room temperature for 15 h and triturated with ether (three times). Yield = 1.457 g (73% based on 3.422 g of **3**). ^{1}H NMR (400 MHz, CD_3OD): δ 4.39 (t, 2H, J = 6.9 Hz, CH_2), 3.2−3.28 (m, 4H, CH_2), 2.82 (t, 2H, J = 8.7 Hz, CH_2). ESI MS m/z: 132.954 (M + H)$^+$/expected m/z value (M + H)$^+$ was 133.098.

Stepwise Assembly of the Acceptor Dye-Labeled Ester Peptide Substrate. Diaminoester (compound **4**) was first labeled with *N*-hydroxysuccinimide (NHS)-activated Alexa Fluor 546 acceptor dye (AFF546-NHS) on one of its constituent primary amines; see step 1 in Figure 2. For this, 4.4 mg of product **4** was dissolved in 300 μL of 2× concentrated phosphate-buffered saline (PBS: 0.276 M NaCl, 0.0054 M KCl, pH 7.4 0.06 M NaH_2PO_4) and added to 1 mg of Alexa Fluor 546 carboxylic acid succinimidyl ester (Life Technologies, Eugene, OR) predissolved in 150 μL of dimethyl sulfoxide (DMSO). Labeling was allowed to proceed overnight on a rotator at room temperature. Given the structure of compound **4**, the dye labeling position on this molecule is nonselective due to the presence of the two flanking amines and we were cognizant that the final product (**5**) would also contain the ester in both possible arrangements. This, however, did not have any noticeable effect on subsequent function (vide infra). Monolabeled AFF546-diaminoester was identified by MS (see data in the SI) and purified by UPLC. The modular, multifunctional peptide (H_6SGP_7NRDRDEDRED, note that this sequence is given C- to N-terminus; obtained from TAG Copenhagen A/S) was then immobilized on a solid phase and activated with a bis(sulfosuccinimidyl)suberate (BS3) cross-linker in step 2 (Figure 2). For this, 2 mg of the peptide (as the trifluoroacetic acid salt) was dissolved in 1 mL of 1× concentrate PBS and then loaded onto 1 mL of Ni^{2+}-nitrilotriacetic acid (Ni^{2+}-NTA) resin (Qiagen, Hilden, Germany) held within an oligonucleotide purification cartridge (OPC) using syringes as described in refs 15 and 16. BS3 (10 mg) dissolved in 1 mL of 1× PBS was then passed back and forth over the peptide-loaded NTA in the OPC for 20 min by hand, and the BS3-activated peptide was washed twice with 10 mL of 1× PBS. The monolabeled AFF546-diaminoester (100 μg) from step 1 dissolved in 1 mL of 1× PBS was then passed over the BS3-activated peptide-loaded NTA by hand for another 20 min and then washed twice with 10 mL of 1× PBS in step 3. The final peptide-BS3-diaminoester-AFF546 crude product was eluted from the Ni^{2+}-NTA resin with five washes of 1 mL 300 mM imidazole in 1× PBS. The eluent was then desalted over reverse-phase C18 media in an OPC, eluted with 70% acetonitrile in H_2O, and concentrated by vacuum.[14,15] The final product (**5**) was identified by MS (see data in the SI), purified by UPLC, quantitated using the dye's molecular extinction coefficient, aliquoted, lyophilized, and stored at −20 °C until individual aliquots were rehydrated in the buffer when needed for experiments.

Substrate Assembly to QDs and Lipase Assay. Aliquots of dye-labeled peptide substrate (**5**) were dissolved in 10 μL of DMSO, then added to 90 μL of assay buffer consisting of 0.1 M NaH_2PO_4, 0.1 M NaCl, pH 4.2, and 0.6% w/w Triton X-100. Stock solutions of the QD sensor construct were typically prepared as follows: for each individual assay point, 25 pmol of 520 nm CL4 QDs were added to 100 pmol of dye-labeled substrate (**5**, ratio of 4 dye-labeled peptide substrates per QD) and allowed to assemble on ice for at least 1 h in the assay buffer. As the constructs were assembling, a dilution curve of lipase was made from a stock solution consisting of 1093 units (U)/mL lipase in a buffer. Utilizing a 384-well plate, 14 μL of the lipase containing solution was added to each well such that the final concentration of lipase ranged in increments from 0.0002 up to 3 U (0.02−314 μM). Prior to starting the kinetic experiment, 11 μL of the QD-construct was added to each well of lipase to a final volume of 25 μL with QD at 0.11 μM (2.75 pmol QD/11 pmol **5**). The plate was immediately inserted in the Tecan Spark plate reader and a kinetic cycle initiated consisting of an interval time of 30 s, exciting at 430 nm, and measuring the fluorescence at 520 nm (QD donor) and 573 nm (AFF546 acceptor).[24] The assay temperature was maintained at 30 °C. To analyze the results, the ratio of the acceptor and the donor PL was determined at each time point for each lipase condition. This ratio was then converted into picomoles of the dye-labeled peptide substrate (**5**) cleaved from the QD utilizing a comparative calibration curve as described in detail in refs 15, 25, and 26. The calibration curve was prepared by assembling the dye-labeled peptide substrate to 520 nm CL4 QD in buffer ranging in ratio from 0 to 6 in a similar manner as that described above.

RESULTS

Sensor Design and Substrate Synthesis. The design, components, and the intended function of the QD displayed lipase sensor is schematically depicted in Figure 1. The sensor consists of central QD scaffolds/donors self-assembled with ratiometric amounts of dye-labeled peptide substrate that display a key ester group recognized by the lipase between the peptidyl and dye portions. When the QD donor is excited, it transfers excitonic energy via FRET to the proximal ground-state acceptor dye; this is directly visualized by a decrease in the QD donor photoluminescence (PL) and an increase in the acceptor dye sensitization. The level of the QD donor PL decrease and concomitant acceptor dye sensitization (i.e., FRET efficiency) is directly proportional to the ratio of acceptor dye-labeled substrate displayed around the QD surface.[10,13,27] In the presence of lipase (CalB), the ester group is recognized and cleaved by the enzyme allowing the acceptor dye to diffuse away from QD proximity and this alters the resulting rate of FRET in a manner that reflects the activity (and concentration) of the enzyme present. The generalized design of this sensor, where a central QD scaffold/donor displays a surrounding acceptor dye-labeled substrate in a quasi-centrosymmetric manner that is then hydrolyzed by a target enzyme during the assay, has been repeatedly implemented for monitoring protease activity.[7]

The key to this sensor's function is the multifunctional dye-labeled peptide substrate whose modular composition provides key properties required for both sensor assembly and function. As shown in the bottom of Figure 2, the peptidyl substrate (compound **5**) consists of four modular components including a peptide, the central C6 spacer originating from a homobifunctional BS3 linker, the diaminoester, and a terminal acceptor dye. The peptidyl portion itself is also modular in nature as highlighted by different colors in Figure 2, top left. The sequence H_6SGP_7NRDRDEDRED-NH_3 (shown C- to N-terminus) consists of five modules in a sequential array including (i) a terminal $(His)_6$ QD attachment module (blue), (ii) an SG flexible linker (purple), (iii) a rigid type II P_7 helix (green), (iv) a NRDRDEDRED charged sequence meant to mimic the cell surface (orange), and (v) the unique N-terminal primary amine (red) that is linked to the rest of the substrate utilizing a BS3 cross-linker. As has been repeatedly shown, terminal attachment to and display of polyhistidine sequences, $(His)_n$, allow proteins, peptides, and even appropriately modified DNA or drugs to self-assemble by metal affinity

https://dx.doi.org/10.1021/acssensors.9b02291
ACS Sens. XXXX, XXX, XXX−XXX

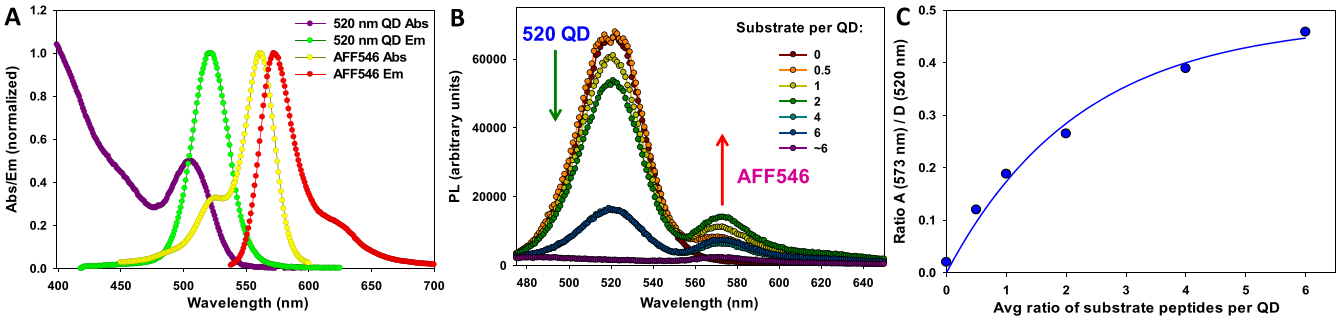

Figure 3. Photophysical properties and calibration curve. (A) Normalized absorption and PL emission of the 520 nm QD donor sample (quantum yield (QY) ~0.25) and the AFF546 acceptor dye (extinction coefficient 112 000 M^{-1} cm^{-1} at 556 nm, $\lambda_{emission\ max}$ 573 nm, QY ~0.5) leading to the spectral overlap of 2.42 × 10^{15} nm^4/M^{-1} cm^{-1} and an R_0 of 4.6 nm. (B) Representative calibration curve where 520 QD donors were assembled with the indicated average ratios of AFF546 dye acceptor-labeled peptide substrate. The sample designated ~6 indicates the acceptor-only control sample at the same concentration as the ratio of 6. Samples were excited at 430 nm, which corresponds to an acceptor absorption minima. (C) A representative plot of the ratio of acceptor PL monitored at 573 nm vs donor PL collected at 520 nm for the data in (B). These data (B, C) act as the calibration curve that allows the conversion of changes in FRET efficiency during a lipase assay to be converted to units of hydrolytic activity.

coordination to the surface of ZnS overcoated QDs as long as the colloidal solubilizing ligand does not preclude the sequence from penetrating through the QDs surrounding the ligand layer.[7,28,29] This high-affinity interaction, K_d ~ 10^{-9} M, is almost spontaneous and typically only requires mixing of the QDs and $(His)_n$-modified moieties in desired stoichiometric amounts. Assembly of the $(His)_6$-peptide to the QDs follows a ratiometric Poisson distribution type process where the display limit is determined by the number of available binding sites on the QD surface; the upper loading limit is expected to be ≥40 peptides/QD for nanocrystals of the current size.[28,30] The SG linker provides some flexibility between the $(His)_6$ QD attachment sequence and the rest of the peptide so that it can bend away and distally extend the rigid $(Pro)_7$ helix spacer away from the QD surface between the surrounding surface ligands that are present. The NRDRDEDRED sequence provides a high level of localized charge near the ester to mimic that typically found on a cell surface. This sequence is drawn from the C-termini of the drug/metabolite transporter (DMT) family of proteins found in Rhodobacteraceae.[31] This sequence was chosen solely for its charge and, similar to the CL4 ligand coating on the QDs, it has a 2:1 ratio between negative and positive charges making it slightly negative. The latter is meant to be reminiscent of the glycocalyx. This combination of sequence and QD ligand represents an a priori attempt at optimization, however, the efficacy would need to be validated in experiments that are beyond the current focus. Lastly, a unique chemical handle in the form of a primary amine is displayed at the peptide's N-terminus to allow for linkage to other functional moieties. Cysteine-thiols are another common handle that is often used as a substitute when the peptide sequence contains more than one primary amine; appropriate homo- and heterobifunctional linkers are available to facilitate this modified linkage as well.[7,15]

The stepwise chemistry used to produce the full peptide–diaminoester–acceptor dye conjugate is detailed in the Materials and Methods section and highlighted in Figure 2 and in the SI. This includes the synthesis of the diaminoester, labeling of one of the amines with AFF546 acceptor dye, and use of solid-phase support to attach the diaminoester-dye to the peptide using a BS3 cross-linker. The correct identity of the final product was confirmed by MS analysis. A full description of all of the other materials and experimental methods utilized can be found in the Materials and Methods section along with the SI.

Assembly of Peptidyl Substrate to the QD, Calibration Curve, and Lipase Assay. For this proof-of-concept demonstration, 520 nm emitting QDs were chosen to be paired with the AFF546 acceptor dye. Figure 3A shows the normalized absorption and emission of both the QD donor and the acceptor confirming that there is substantial spectral overlap present in this system, which has a predicted Förster distance or R_0 of ~4.6 nm corresponding to the donor–acceptor separation distance where FRET at 50% energy transfer efficiency will occur.[10,13,27] The resulting spectroscopic data plot shown in Figure 3B confirms that the AFF546 acceptor dye-labeled peptidyl substrate does indeed assemble to the 520 nm QD. As the ratio of peptidyl substrate per QD is increased stepwise from 0.5 up to 6, the QD donor PL is substantially quenched while that of the acceptor increases concomitantly. This occurs as expected since the increasing presence of acceptor dye centrosymmetrically displayed around the QD donor increases the acceptor's absorption cross section (i.e., its cumulative molecular extinction coefficient) and this results in a proportional increase in the resulting FRET efficiency, which directly tracks with the ratio of acceptor present per QD.[13] Utilizing the calibration curve, an average donor–acceptor distance of 5.7 ± 0.6 nm was determined. For QD scaffolded systems, it is generally considered that the donor dipole is situated at the center of the QD; considering the QD radius of ~2.7 nm, this suggests that the dye projects around 3 nm away from the QD surface.[13] As seen in Figure 3B, an acceptor-only control sample of 6 equivalents (~6) substrate alone directly excited at the same 430 nm wavelength, which corresponds to an AFF546 absorption minima with only a predicted ~2% direct excitation component, confirms that the AFF546 signal is almost all attributable to FRET sensitization of the acceptor by the QD donor. This can actually be quite helpful as it simplifies both the initial generation of the calibration curve and subsequent data analysis by removing the requirement to account for any direct excitation of the acceptor.[15,32]

This same "FRET titration" also serves as a calibration curve to convert changes in acceptor–donor PL ratios due to hydrolytic cleavage of the ester by lipase into the amount or concentration of substrate cleaved over time. Rather than tracking QD donor loss or acceptor sensitization alone for this

https://dx.doi.org/10.1021/acssensors.9b02291
ACS Sens. XXXX, XXX, XXX–XXX

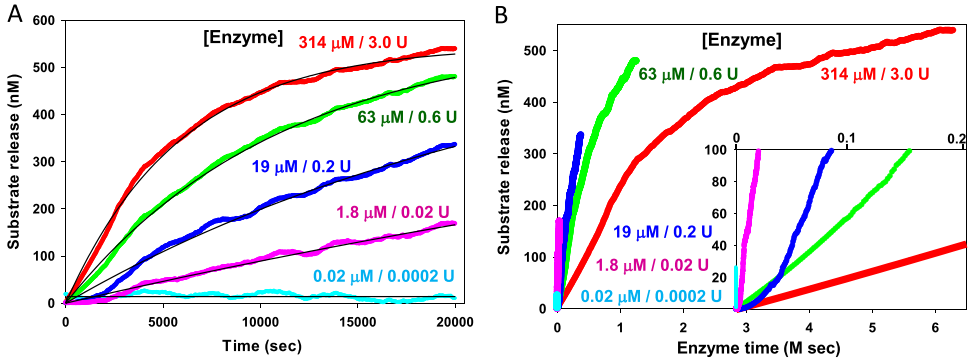

Figure 4. Progress curves from lipase assay with the QD-peptide ester substrate. (A) 520 QDs were assembled with an average ratio of 4 AFF546 acceptor-labeled peptidyl substrates per QD and assayed against increasing concentrations of CalB ranging from 0.02 up to 314 μM over time as indicated. The corresponding number of units of CalB present per assay is shown in the plot. The ratio of AFF546 acceptor to QD donor PL was then converted into an overall substrate release using the calibration curve in Figure 3C. (B) Progress curves in enzyme time for the data shown in (A). The inset focuses in on earlier time points to highlight the initial components of the progress curves for the lower enzyme concentrations. The corresponding number of units of CalB present per assay is shown in the plot.

metric, the use of an acceptor/donor ratio is preferred in generalized biosensing formats since it is far more robust to issues arising from relative concentration and instrumental variation.[10,12,13] Figure 3C plots the ratio of acceptor−donor PL for the data shown in Figure 3B and these data are then fitted with an exponential growth function to yield an equation that allows ratio values in the specified range to be directly converted into the corresponding number of substrate peptides per QD as described.[15,25,26]

To test this sensor format in a proof-of-concept assay, the peptidyl substrate was assembled to 520 QD at an average ratio of 4 substrates per QD; this ratio was specifically chosen as it is well within the upper boundary of six acceptor-labeled substrates used in the calibration curve. Assay volumes of 25 μL were utilized containing 0.11 μM QD (displaying 0.44 μM peptide substrate) and exposed to increasing concentrations of CalB ranging from 0.02 up to 314 μM, as shown in Figure 4. PL was monitored over time simultaneously at 573 nm (acceptor) and 520 nm (donor) and the resulting ratio values converted to the number of peptide substrates remaining attached to the QD vs time. This, in turn, was converted into the concentration of the substrate released, as shown in Figure 4A. Here, all enzyme concentrations, except the lowest of 0.02 μM resulted in the appreciable release of the substrate from the QD.

Michaelis−Menten Analysis. Although the appearance of the resulting enzymatic progress curve data plots is reminiscent of that collected from classical enzyme assay formats, extracting the corresponding standard Michaelis−Menten (MM) kinetic descriptors from this data is not as straightforward. This arises from the fact that the amount of enzyme in the assay is in excess of the substrate and thus this format does not meet the standard Briggs−Haldane steady-state assumption of ($d[ES]/dt = 0$), where E is the enzyme and S is the substrate, which is usually achieved when $[S] \gg [E]$.[26,33,34] However, an integrated version of the MM can be implemented to yield the time-dependent substrate concentration $[S]_t$ in terms of the Michaelis constant (K_M), catalytic rate (k_{cat}) enzyme velocity (V), initial substrate concentration $[S]_0$, and time (t) using[15,26,33,35]

$$K_M \ln\left(\frac{[S]_0}{[S]_t}\right) + ([S]_0 - [S]_t) = Vt \quad (1)$$

and

$$V = k_{cat} \times [E] \quad (2)$$

It is important to note that this was the very methodology utilized by Michaelis and Menten in their seminal studies.[36] This approach is predicated on the validity of several underlying mechanistic assumptions that include (i) the reaction is nonreversible, (ii) the enzyme is stable over time, and (iii) the product does not act as an inhibitor.[35] Moreover, reliably estimating individual K_M and k_{cat} values from these type of progress data requires that other criteria are satisfied including (iv) $[S]_0 > K_M$ and (v) Selwyn's test.[37] If criterion (iv) is not satisfied, then the progress curves will only reflect the ratio of k_{cat}/K_M; this effective second-order rate constant is commonly called the specificity constant and is quite useful as a common measure of enzyme efficiency in and of itself.[33,37] Given the K_M determined for CalB below, the corresponding amount of QD substrate required to achieve $[S]_0 > K_M$ would be in the millimolar range which is not a realistically attainable assay concentration achievable with colloidal QDs nor can FRET be monitored real time in that scenario due to substantial signal scattering.[10,27] Selwyn's test indicates that the progress curves from a system obeying a classic MM kinetic process when implemented with a fixed $[S]_0$ and variable $[E]_0$ should superimpose over each other when time is scaled by $[E]_0$ to provide for a common trajectory in so-called "enzyme time" ($[E]_0 t$ described in units of molar second).[37]

To determine a comparative baseline for the enzyme's kinetic activity in this buffer, we assayed the CalB native activity using a commercial chromogenic 4-nitrophenyl palmitate (NPPL) lipase substrate in a standard fixed enzyme, increasing excess substrate format where $[S] \gg [E]$.[26,33,34] This yielded an estimated K_M of 1066 ± 268 μM, k_{cat} of 0.42 ± 0.18 min^{-1}, and a k_{cat}/K_M of 0.41 ± 0.20 min^{-1} mM^{-1} (data not shown).[38] This compares quite favorably with some representative reported values for K_M of 410 ± 410 and 484 ± 11 μM (both with *p*-nitrophenol butyrate substrate), a k_{cat} of 2 ± 0.1 min^{-1} (6.8-difluoro-4-methylumbelliferyl or DiFMU octanoate substrate) or 16 ± 1 min^{-1} (*p*-nitrophenol butyrate), and a k_{cat}/K_M of 0.8 × 10^{-3} min^{-1} mM^{-1} (DiFMU octanoate) or 33 × 10^{-3} min^{-1} mM^{-1} reported for wild type recombinant CalB expressed in either *Pichia pastoris* or *A. oryzae*.[38,39]

https://dx.doi.org/10.1021/acssensors.9b02291
ACS Sens. XXXX, XXX, XXX−XXX

Since our assay format does not satisfy criteria (iv) ($[S]_0 > K_M$) above, we utilized the integrated MM approach of eq 1 to estimate an averaged k_{cat}/K_M of 421 ± 81 min^{-1} mM^{-1} from the assay data in Figure 4A. This appears to be orders of magnitude more efficient than that reported for the same enzyme with solution-phase DiFMU octanoate albeit with a far different substrate architecture—that of multiple copies of an ester-containing target molecule displayed around a central QD. Figure 4B presents the same data but now converted into enzyme time, with the inset highlighting the activity of the lower enzyme concentrations over a smaller range. From these plots, it is apparent that the activities of all of the different enzyme concentrations do not superimpose over each other, even when considering the earliest time points. We also note that the minimal measurable activity (MMA) for enzyme activity corresponded to 0.0002 U using an experimental format based on serial dilutions (within the time frame tested) and that this also matched with that seen for the NPPL substrate with a free enzyme (data not shown).

DISCUSSION AND CONCLUSIONS

We have previously reported on an analogous sensor design that targeted protease activity and was analyzed using the same approach due to the same enzyme vs substrate concentration issues, i.e., [S] ≫ [E] was not achievable.[26] In that investigation, a series of dye-labeled peptides were self-assembled at increasing average ratios ranging from 2.4 up to 13.4 per QD to yield the assembled biosensor, which was implemented at 0.5 μM concentration. Trypsin proteolysis was targeted in this configuration and the results indicated that enzyme efficiency (k_{cat}/K_M) increased ca. 5-fold when the peptide was displayed around a QD as compared to free in solution. When plotted in the form of enzyme time progress curves (analogous to that presented in Figure 4B), the assay data itself superimposed at earlier time points suggesting that the activity obeyed a classic MM kinetic process initially and then deviated; supporting this conclusion, the curves could not be fit to a MM model especially at later time points. More importantly, Algar showed that the data were consistent with a "hopping" model of enzyme activity where trypsin interacted with a given QD-peptide substrate, consumed all of the peptide displayed around that QD, and then diffused away to encounter another substrate.[26] A similar model has been recently reported for DNAse activity on a DNA-coated protein.[40] The other models considered as potential contributors to the observed trypsin activity included a classical MM model, where the enzyme interacted with one peptide substrate displayed on the QD, cleaved it and diffused away, and a scooting model where the enzyme hydrolyzed all of the substrate presented around a given QD in a rapid fashion but never left that surface again. Interestingly, the latter model is derived from that of lipase activity on cell surfaces (vide infra).[2,41−43] Algar has subsequently significantly expanded the limits of this overall sensor design in a series of elegant reports revealing how the physicochemical properties of the QD surface ligand influence the hopping activity along with showing that it is inherently amenable to multiplexed analysis targeting two or even up to three different proteases at the same time.[25,44−48] He has even utilized it to monitor the activity of one enzyme (trypsin) activating another (chymotrypsin) when the second is present in its nascent inactive proform.[49] It is quite likely that many of the same functional mechanisms and associated limitations found within the above-described protease sensors are also at play in the current QD-based lipase biosensing format.

Lipases, in general, are characterized by an unusual protein structure, which then gives rise to unique modes of activity that are not normally found in other superfamilies of hydrolytic enzymes.[8,41,43,50] The functional structure of most lipases, including CalB, is characterized by the presence of a hinged lid that is located covering their catalytic site.[2,38,41,42,51] This unusual structure is suggested to allow them to function at the lipid−water interface since lipid hydrophobicity induces the opening of the lid and access to the catalytic triad via interfacial activation. Moreover, in a purely aqueous buffer, the lid does not open and the enzyme is not active, while the addition of some percentage of organic solvent can activate the enzyme. This makes these enzymes especially useful in commercial trans-esterification and other related types of catalysis.[4,5,43] The kinetics of these enzymes on small molecule substrates such as NPPL are assumed to follow MM kinetic processes and their values are estimated using the standard MM formulae as described in the literature.[38,39] However, it is also strongly argued that in the context of a cellular surface displaying lipidic substrate, lipases will interact with the cell membrane and hydrolyze the substrate by utilizing a scooting mode of activity, which also has a strong dependence on enzyme affinity for the cell surface.[6,41,42,50] This essentially reduces the activity of the enzyme to a localized surface in this context, which cannot be easily described with the standard MM model, that is based on the interactions of diffusional components.[2,33,41,42]

The results shown in Figure 4B, where CalB activity was converted into enzyme time and where the different enzyme trajectories do not superimpose over each other, support the idea of a nonclassical MM process underlying the observed activity. If the process followed that expected for standard MM interactions, then these lines (i.e., trajectories) should all have superimposed over each other in the plots. This could potentially arise from the enzyme displaying its scooting mode of activity in conjunction with it having an interfacial affinity for both the QD surface ligand and the displayed substrate. At the pH of the buffer utilized, the peptide is predicted to have a net charge of +7 while that of the CalB is +13, which would preclude purely electrostatic interactions between these two entities. In contrast, the QD's CL4 ligand will have a negatively charged component and this could potentially interact with the positively charged CalB in a manner similar to that shown for other proteases interacting with similar peptide substrate displaying QDs.[52] It is also probable that the QD's extremely high surface-to-volume ratio (∼1.1) as compared to that of a typical cellular surface could play an influential role as well. Moreover, the CalB affinity for the QD substrate construct and its apparent activity could change based on the remaining number of peptidyl-ester substrates displayed around it in a manner akin to that shown for DNAse activity on DNA-coated proteins.[40] One experimental approach to elucidating the roles of each of these potentially contributing factors would be to perform the same type of experiments with a series of increasingly larger NPs.[23] This would most likely require switching to another nanoparticulate material with wider size diversity such as gold NPs, for example, as accessible QD size diversity is quite narrowly restricted to a smaller range in comparison given their inherent compositional, synthetic chemistry, and quantum confinement properties. Following on the example of Algar[44,45,47] and others,[52] performing assays utilizing QDs surface-function-

https://dx.doi.org/10.1021/acssensors.9b02291
ACS Sens. XXXX, XXX, XXX−XXX

alized with different ligands ranging from polar to slightly hydrophilic could be quite insightful about some of the underlying interactions, which influence the mechanics of this process. Moreover, molecular dynamic modeling of these interactions could provide useful information about the CalB–QD surface interactions in this context.[52] It is worth noting that these types of experiments are not trivial and typically require several years of material preparation and time investment. We also note another important and confounding issue which is not often taken into account when dealing with biological interactions at a nanoparticulate material interface. That is, the recent finding that nanoparticles universally structure the solvent that surrounds them and this gives rise to a localized physicochemical environment at the particles' interface, which is not well understood but which is believed to be characterized by a boundary, solvent, and ionic gradients and changes in density among other properties.[53,54] This unique environment has already been shown to directly influence enzyme activity by productively altering rate-limiting steps.[23]

Overall, the current report provides proof-of-concept for an alternative lipase biosensing format based on a NP display architecture that is reminiscent of lipase activity on a cell surface. One potential limitation of this design arises from the peptidyl segment itself, which would make the construct responsive to protease activity such as that of trypsin and other proteases that recognize and cleave residues or short sequences that may be incorporated therein.[15,16,55] From an analytical perspective, this would require making sure that such enzymes are not inadvertently added with lipase for an assay as both classes of enzymes are jointly present in detergents and other food preparation processes.[4,5] Nevertheless, this biosensor suggests itself as being potentially quite useful toward helping elucidate many of the complex, yet subtle characteristics of this important enzyme family. Future studies will focus on understanding the mechanisms that control the initial interactions between enzyme and QD substrate along with subsequent kinetic activity, including especially NP size, and then using this insight to design optimized second-generation lipase sensors for further application. Additionally, experiments with this optimized QD sensor within a single-molecule fluorescence modality would certainly help elucidate its catalytic processes on these type of nanoscale scaffolds.[56,57]

■ ASSOCIATED CONTENT

Supporting Information

The Supporting Information is available free of charge at https://pubs.acs.org/doi/10.1021/acssensors.9b02291.

Synthetic intermediaries and final diaminoester product; chemical structure of the CL4 ligand used to make the QDs colloidally stable; mass-spectral confirmation of synthetic intermediaries and products; compound **4** purification and identification; AFF546-labeled compound **4** purification and analysis; compound **5** purification and analysis (PDF)

■ AUTHOR INFORMATION

Corresponding Author

Igor L. Medintz − *Center for Bio/Molecular Science and Engineering, U.S. Naval Research Laboratory, Washington, District of Columbia 20375, United States;* orcid.org/0000-0002-8902-4687; Email: Igor.medintz@nrl.navy.mil

Authors

Joyce C. Breger − *Center for Bio/Molecular Science and Engineering, U.S. Naval Research Laboratory, Washington, District of Columbia 20375, United States*

Kimihiro Susumu − *Optical Sciences Division, U.S. Naval Research Laboratory, Washington, District of Columbia 20375, United States; KeyW Corporation, Hanover, Maryland 21076, United States;* orcid.org/0000-0003-4389-2574

Guillermo Lasarte-Aragonés − *Center for Bio/Molecular Science and Engineering, U.S. Naval Research Laboratory, Washington, District of Columbia 20375, United States; Department of Bioengineering, George Mason University, Fairfax, Virginia 22030, United States;* orcid.org/0000-0003-3502-9367

Sebastián A. Díaz − *Center for Bio/Molecular Science and Engineering, U.S. Naval Research Laboratory, Washington, District of Columbia 20375, United States;* orcid.org/0000-0002-5568-0512

Jesper Brask − *Novozymes A/S, 2800 Kgs. Lyngby, Denmark*

Complete contact information is available at: https://pubs.acs.org/10.1021/acssensors.9b02291

Notes

The authors declare no competing financial interest.

■ ACKNOWLEDGMENTS

I.L.M. acknowledges support from ONR, NRL, the NRL Nanosciences Institute, and USDA Grant No. 2016-67021-25038.

■ REFERENCES

(1) Scrutton, N. *Enzymes in Synthetic Biology*; Elsevier: The Netherlands, 2018; Vol. *608*.

(2) Reis, P.; Holmberg, K.; Watzke, H.; Leser, M. E.; Miller, R. Lipases at Interfaces: A Review. *Adv. Colloid Interface Sci.* **2009**, *147–148*, 237–250.

(3) Hube, B.; Stehr, F.; Bossenz, M.; Mazur, A.; Kretschmar, M.; Schafer, W. Secreted Lipases of *Candida albicans*: Cloning, Characterisation and Expression Analysis of a New Gene Family with at Least Ten Members. *Arch. Microbiol.* **2000**, *174*, 362–374.

(4) Ribeiro, B. D.; de Castro, A. M.; Coelho, M. A. Z.; Freire, D. M. G. Production and Use of Lipases in Bioenergy: A Review from the Feedstocks to Biodiesel Production. *Enzyme Res.* **2011**, *2011*, No. 615803.

(5) Guerrand, D. Lipases Industrial Applications: Focus on Food and Agroindustries. *Oilseeds, fats, Corps Lipids* **2017**, *24*, No. D403.

(6) Grabner, G. F.; Zimmermann, R.; Schicho, R.; Taschler, U. Monoglyceride Lipase as a Drug Target: At the Crossroads of Arachidonic Acid Metabolism and Endocannabinoid Signaling. *Pharmacol. Ther.* **2017**, *175*, 35–46.

(7) Nagy, A.; Gemmill, K. B.; Delehanty, J. B.; Medintz, I. L.; Sapsford, K. E. Peptide-Functionalized Quantum Dot Biosensors. *IEEE J. Sel. Top. Quantum Electron.* **2014**, *20*, No. 6900512.

(8) Chahiniana, H.; Sarda, L. Distinction between Esterases and Lipases: Comparative Biochemical Properties of Sequence-Related Carboxylesterases. *Protein Pept. Lett.* **2009**, *16*, 1149–1161.

(9) Heeren, J.; Bruns, O. Nanocrystals, a New Tool to Study Lipoprotein Metabolism and Atherosclerosis. *Curr. Pharm. Biotechnol.* **2012**, *13*, 365–372.

(10) Algar, W. R.; Hildebrandt, N.; Vogel, S. S.; Medintz, I. L. FRET as a Biomolecular Research Tool-Understanding It's Potential While Avoiding Pitfalls. *Nat. Methods* **2019**, *16*, 815–829.

(11) Huang, H. T.; Garu, P.; Li, C. H.; Chang, W. C.; Chen, B. W.; Sung, S. Y.; Lee, C. M.; Chen, J. Y.; Hsieh, T. F.; et al. Magnetoresistive Biosensors for Direct Detection of Magnetic

Nanoparticle Conjugated Biomarkers on a Chip. *Spin* **2019**, *9*, No. 19400022.
(12) Walper, S. A.; Aragones, G. L.; Sapsford, K. E.; Brown, C. W.; Rowland, C. E.; Breger, J. C.; Medintz, I. L. Detecting Biothreat Agents: From Current Diagnostics to Developing Sensor Technologies. *ACS Sens.* **2018**, *3*, 1894−2024.
(13) Hildebrandt, N.; Spillmann, C. M.; Algar, W. R.; Pons, T.; Stewart, M. H.; Oh, E.; Susumu, K.; Diaz, S. A.; Delehanty, J. B.; Medintz, I. L. Energy Transfer with Semiconductor Quantum Dot Bioconjugates: A Versatile Platform for Biosensing, Energy Harvesting, and Other Developing Applications. *Chem. Rev.* **2017**, *117*, 536−711.
(14) Hu, J.; Li, Y.; Li, Y.; Tang, B.; Zhang, C.-Y. Single Quantum Dot-Based Nanosensor for Sensitive Detection of O-GlcNAc Transferase Activity. *Anal. Chem.* **2017**, *89*, 12992−12999.
(15) Díaz, S. A.; Breger, J. C.; Medintz, I. L. Monitoring Enzymatic Proteolysis Using Either Enzyme- or Substrate-Bioconjugated Quantum Dots. *Methods Enzymol.* **2016**, *571*, 19−54.
(16) Sapsford, K. E.; Farrell, D.; Sun, S.; Rasooly, A.; Mattoussi, H.; Medintz, I. L. Monitoring of Enzymatic Proteolysis on a Electroluminescent-CCD Microchip Platform Using Quantum Dot-Peptide Substrates. *Sens. Actuators, B* **2009**, *139*, 13−21.
(17) Zhang, W.; Liu, J.; Zhang, L.; Gan, J.-H.; Ding, Y.; Huang, W.; Huo, F.-W.; Tian, D. A Fluorescence Nanosensor for Lipase Activity: Enzyme-Regulated Quantum Dots Growth in situ. *RSC Adv.* **2015**, *5*, 73051−73057.
(18) Susumu, K.; Field, L. D.; Oh, E.; Hunt, M.; Delehanty, J. B.; Palomo, V.; Dawson, P. E.; Huston, A. L.; Medintz, I. L. Purple-, Blue-, and Green-Emitting Multishell Alloyed Quantum Dots: Synthesis, Characterization, and Application for Ratiometric Extracellular pH Sensing. *Chem. Mater.* **2017**, *29*, 7330−7344.
(19) Susumu, K.; Oh, E.; Delehanty, J. B.; Blanco-Canosa, J. B.; Johnson, B. J.; Jain, V.; Hervey, W. J.; Algar, W. R.; Boeneman, K.; Dawson, P. E.; Medintz, I. L. Multifunctional Compact Zwitterionic Ligands for Preparing Robust Biocompatible Semiconductor Quantum Dots and Gold Nanoparticles. *J. Am. Chem. Soc.* **2011**, *133*, 9480−9496.
(20) Susumu, K.; Oh, E.; Delehanty, J. B.; Pinaud, F.; Gemmill, K. B.; Walper, S.; Breger, J.; Schroeder, M. J.; Stewart, M. H.; Jain, V.; Whitaker, C. M.; et al. A New Family of Pyridine-Appended Multidentate Polymers As Hydrophilic Surface Ligands for Preparing Stable Biocompatible Quantum Dots. *Chem. Mater.* **2014**, *26*, 5327−5344.
(21) Gemmill, K. B.; Díaz, S.; Blanco-Canosa, J. B.; Deschamps, J. R.; Pons, T.; Liu, H.-W.; Deniz, A.; Melinger, J.; Oh, E.; Susumu, K.; Stewart, M.; Hastman, D.; North, S.; Delehanty, J. B.; Dawson, P.; Medintz, I. L. Examining the Polyproline Nanoscopic Ruler in the Context of Quantum Dots. *Chem. Mater.* **2015**, *27*, 6222−6237.
(22) Díaz, S. A.; Lasarte-Aragones, G.; Lowery, R. G.; Aniket; Vranish, J. N.; Klein, W. P.; Susumu, K.; Medintz, I. L. Quantum Dots as Förster Resonance Energy Transfer Acceptors of Lanthanides in Time-Resolved Bioassays. *ACS Appl. Nano Mater.* **2018**, *1*, 3006−3014.
(23) Breger, J. C.; Oh, E.; Susumu, K.; Klein, W. P.; Walper, S. A.; Ancona, M. G.; Medintz, I. L. Nanoparticle Size Influences Localized Enzymatic Enhancement-A Case Study with Phosphotriesterase. *Bioconjugate Chem.* **2019**, *30*, 2060−2074.
(24) Gemmill, K. B.; Deschamps, J. R.; Delehanty, J. B.; Susumu, K.; Stewart, M. H.; Glaven, R. H.; Anderson, G. P.; Goldman, E. R.; Huston, A. L.; Medintz, I. L. Optimizing Protein Coordination to Quantum Dots with Designer Peptidyl Linkers. *Bioconjugate Chem.* **2013**, *24*, 269−281.
(25) Algar, W. R.; Malanoski, A. P.; Susumu, K.; Stewart, M. H.; Hildebrandt, N.; Medintz, I. L. Multiplexed Tracking of Protease Activity Using a Single Color of Quantum Dot Vector and a Time-Gated Forster Resonance Energy Transfer Relay. *Anal. Chem.* **2012**, *84*, 10136−10146.
(26) Algar, W. R.; Malonoski, A.; Deschamps, J. R.; Banco-Canosa, J. B.; Susumu, K.; Stewart, M. H.; Johnson, B. J.; Dawson, P. E.; Medintz, I. L. Proteolytic Activity at Quantum Dot-Conjugates: Kinetic Analysis Reveals Enhanced Enzyme Activity and Localized Interfacial "Hopping". *Nano Lett.* **2012**, *12*, 3793−3802.
(27) Medintz, I. L.; Hildebrandt, N. *FRET—Förster Resonance Energy Transfer From Theory to Applications*; Wiley-VCH: Weinheim, Germany, 2013.
(28) Blanco-Canosa, J. B.; Wu, M.; Susumu, K.; Petryayeva, E.; Jennings, T. L.; Dawson, P. E.; Algar, W. R.; Medintz, I. L. Recent Progress in the Bioconjugation of Quantum Dots. *Coord. Chem. Rev.* **2014**, *263*−*264*, 101−137.
(29) Gemmill, K. B.; Muttenthaler, M.; Delehanty, J. B.; Stewart, M. H.; Susumu, K.; Dawson, P. E.; Medintz, I. L. Evaluation of Diverse Peptidyl Motifs for Cellular Delivery of Semiconductor Quantum Dots. *Anal. Bioanal. Chem.* **2013**, *405*, 6145−6154.
(30) Prasuhn, D. E.; Deschamps, J. R.; Susumu, K.; Stewart, M. H.; Boeneman, K.; Blanco-Canosa, J. B.; Dawson, P. E.; Medintz, I. L. Polyvalent Display and Packing of Peptides and Proteins on Semiconductor Quantum Dots: Predicted Versus Experimental Results. *Small* **2010**, *6*, 555−564.
(31) Arahal, D. R.; Pujalte, M. J.; Rodrigo-Torres, L. Draft Genomic Sequence of *Nereida ignava* CECT 5292(T), A Marine Bacterium of the Family *Rhodobacteraceae*. *Stand. Genomic Sci.* **2016**, *11*, No. 21.
(32) Díaz, S. A.; Malonoski, A. P.; Susumu, K.; Hofele, R. V.; Oh, E.; Medintz, I. L. Probing the Kinetics of Quantum Dot-Based Proteolytic Sensors. *Anal. Bioanal. Chem.* **2015**, *407*, 7307−7318.
(33) Cornish-Bowden, A. *Fundamentals of Enzyme Kinetics*, 4th ed.; Wiley-Blackwell: Winheim, Germany, 2012.
(34) Briggs, G. E.; Haldane, J. B. S. A Note on the Kinetics of Enzyme Actions. *Biochem. J.* **1925**, *19*, 338−339.
(35) Marangoni, A. G. *Enzyme Kinetics: A Modern Approach*; John Wiley & Sons, Inc.: Hoboken, NJ, 2003.
(36) Johnson, K. A.; Goody, R. S. The Original Michaelis Constant: Translation of the 1913 Michaelis-Menten Paper. *Biochemistry* **2011**, *50*, 8264−8269.
(37) Duggleby, R. G.; Clarke, R. B. Experimental-Designs for Estimating The Parameters of the Michaelis-Menten Equation From Progress Curves of Enzyme-Catalyzed Reactions. *Biochim. Biophys. Acta, Protein Struct. Mol. Enzymol.* **1991**, *1080*, 231−236.
(38) Skjøt, M.; De Maria, L.; Chatterjee, R.; Svendsen, A.; Patkar, S. A.; Østergaard, P. R.; Brask, J. Understanding the Plasticity of the alpha/beta Hydrolase Fold: Lid Swapping on the *Candida antarctica* Lipase B Results in Chimeras with Interesting Biocatalytic Properties. *ChemBioChem* **2009**, *10*, 520−527.
(39) Qian, Z.; Lutz, S. Improving the Catalytic Activity of *Candida antarctica* Lipase B by Circular Permutation. *J. Am. Chem. Soc.* **2005**, *127*, 13466−13467.
(40) Krishnamoorthy, K.; Kewalramani, S.; Ehlen, A.; Moreau, L. M.; Mirkin, C. A.; de la Cruz, M. O.; Bedzyk, M. J. Enzymatic Degradation of DNA Probed by In Situ X-ray Scattering. *ACS Nano* **2019**, *13*, 11382−11391.
(41) Gelb, M. H.; Jain, M. K.; Hanel, A. M.; Berg, O. G. Interfacial Enzymology of Glycerolipid Hydrolases − Lessons from Secreted Phospholipases A(2). *Ann. Rev. Biochem.* **1995**, *64*, 653−688.
(42) Khan, F. I.; Lan, D.; Durrani, R.; Huan, W.; Zhao, Z.; Wang, Y. The Lid Domain in Lipases: Structural and Functional Determinant of Enzymatic Properties. *Front. Bioeng. Biotechnol.* **2017**, *5*, No. 16.
(43) Schmid, R. D.; Verger, R. Lipases: Interfacial Enzymes with Attractive Applications. *Angew. Chem., Int. Ed.* **1998**, *37*, 1609−1633.
(44) Jeen, T.; Algar, W. R. Mimicking Cell Surface Enhancement of Protease Activity on the Surface of a Quantum Dot Nanoparticle. *Bioconjugate Chem.* **2018**, *29*, 3783−3792.
(45) Algar, W. R.; Jeen, T.; Massey, M.; Peveler, W. J.; Asselin, J. Small Surface, Big Effects, and Big Challenges: Toward Understanding Enzymatic Activity at the Inorganic Nanoparticle-Substrate Interface. *Langmuir* **2019**, *35*, 7067−7091.
(46) Massey, M.; Kim, H.; Conroy, E. M.; Algar, W. R. Expanded Quantum Dot-Based Concentric Forster Resonance Energy Transfer: Adding and Characterizing Energy-Transfer Pathways for Triply Multiplexed Biosensing. *J. Phys. Chem. C* **2017**, *121*, 13345−13356.

https://dx.doi.org/10.1021/acssensors.9b02291
ACS Sens. XXXX, XXX, XXX−XXX

(47) Petryayeva, E.; Jeen, T.; Algar, W. R. Optimization and Changes in the Mode of Proteolytic Turnover of Quantum Dot-Peptide Substrate Conjugates through Moderation of Interfacial Adsorption. *ACS Appl. Mater. Interfaces* **2017**, *9*, 30359−30372.
(48) Wu, M.; Algar, W. R. Acceleration of Proteolytic Activity Associated with Selection of Thiol Ligand Coatings on Quantum Dots. *ACS Appl. Mater. Interfaces* **2015**, *7*, 2535−2545.
(49) Algar, W. R.; Ancona, M. G.; Malanoski, A. P.; Susumu, K.; Medintz, I. L. Assembly of a Concentric Forster Resonance Energy Transfer Relay on a Quantum Dot Scaffold: Characterization and Application to Multiplexed Protease Sensing. *ACS Nano* **2012**, *6*, 11044−11058.
(50) Verger, R. 'Interfacial Activation' of Lipases: Facts and Artifacts. *Trends Biotechnol.* **1997**, *15*, 32−38.
(51) Stauch, B.; Fisher, S. J.; Cianci, M. Open and Closed States of *Candida antarctica* Lipase B: Protonation and the Mechanism of Interfacial Activation. *J. Lipid Res.* **2015**, *56*, 2348−2358.
(52) Díaz, S. A.; Sen, S.; Gemmill, K. B.; Brown, C. W.; Oh, E.; Susumu, K.; Stewart, M. H.; Breger, J. C.; Aragones, G. L.; Field, L. D.; et al. Elucidating Surface Ligand-Dependent Kinetic Enhancement of Proteolytic Activity at Surface-Modified Quantum Dots. *ACS Nano* **2017**, *11*, 5884−5896.
(53) Vranish, J. N.; Ancona, M. G.; Walper, S. A.; Medintz, I. L. Pursuing the Promise of Enzymatic Enhancement with Nanoparticle Assemblies. *Langmuir* **2018**, *34*, 2901−2925.
(54) Zobel, M.; Neder, R. B.; Kimber, S. A. J. Universal Solvent Restructuring Induced By Colloidal Nanoparticles. *Science* **2015**, *347*, 292−294.
(55) Algar, W. R.; Blanco-Canosa, J. B.; Manthe, R. L.; Susumu, K.; Stewart, M. H.; Dawson, P. E.; Medintz, I. L. Synthesizing and Modifying Peptides for Chemoselective Ligation and Assembly into Quantum Dot-Peptide Bioconjugates. In *Nanomaterial Interfaces in Biology*; Bergese, P.; Hamad-Schifferli, K., Eds.; Methods in Molecular Biology; Humana Press: Totowa, NJ, 2013; Vol. *1025*, pp 47−73.
(56) Wang, L.-J.; Luo, M.-L.; Zhang, Q.; Tang, B.; Zhang, C.-Y. Single Quantum Dot-Based Nanosensor for Rapid and Sensitive Detection of Terminal Deoxynucleotidyl Transferase. *Chem. Commun.* **2017**, *53*, 11016−11019.
(57) Ma, F.; Li, Y.; Tang, B.; Zhang, C.-Y. Fluorescent Biosensors Based on Single-Molecule Counting. *Acc. Chem. Res.* **2016**, *49*, 1722−1730.

https://dx.doi.org/10.1021/acssensors.9b02291
ACS Sens. XXXX, XXX, XXX−XXX